Energy Conversion and Management: X 29 (2026) 101494

Contents lists available at ScienceDirect

Energy Conversion and Management: X

journal homepage: www.sciencedirect.com/journal/energy-conversion-and-management-x

Kinetic, thermodynamic, and process evaluation of Dracaena draco biomass fiber pyrolysis for sustainable biofuel production

Abdelwaheb Hadou [a], Ahmed Belaadi [a,*], Aghilas Brahmi [b], Messaouda Boumaaza [c], Mohammad Jawaid [d,e,**], Djamel Ghernaout [f,g], Vincenzo Fiore [h]

[a] Department of Mechanical Engineering, Faculty of Technology, University 20 August 1955-Skikda, El-Hadaiek, Skikda, Algeria
[b] Laboratoire des Matériaux et Développement Durable (LMDD), Département de Génie des Procédés, Faculté des Sciences Appliquées, Université de Bouira, 10000, Algeria
[c] Laboratory of Civil Engineering and Hydraulics (LGCH), University 8 May 1945 Guelma, PO Box 401, Guelma 24000, Algeria
[d] Department of Chemical and Petroleum Engineering, College of Engineering, United Arab Emirates University, PO Box 15551, Al Ain, United Arab Emirates
[e] National Water and Energy Center, United Arab Emirates University, PO Box 15551, Al Ain, United Arab Emirates
[f] Chemical Engineering Department, College of Engineering, University of Ha'il, PO Box 2440, Ha'il 81441, Saudi Arabia
[g] Chemical Engineering Department, Faculty of Engineering, University of Blida, PO Box 270, Blida 09000, Algeria
[h] Department of Engineering, University of Palermo, Viale delle Scienze, Building 6, 90128 Palermo, Italy

ARTICLE INFO

Keywords:
Dracaena draco waste fibers pyrolysis
Pyrolysis Kinetics
Coats–Redfern method
Renewable biofuel production
Biomass valorization

ABSTRACT

As global demand for sustainable energy intensifies, the depletion of fossil fuels and environmental concerns drive the search for alternative, renewable resources. Biomass, particularly underutilized waste fibers, offers significant potential. This study investigates Dracaena draco waste fibers (DdwFs) as a promising feedstock for biofuel production through pyrolysis, a well-established thermochemical process.Using thermogravimetric (TGA) analysis at heating rates of 15, 25, and 30 °C min^{-1}, the study examines the pyrolysis kinetics and thermodynamics of DdwFs. The Coats–Redfern method is applied to determine the kinetic triplet, activation energy (E_a), pre-exponential factor (A), and reaction mechanism, while Criado's master plot validates the model. The results reveal a multi-step degradation process involving hemicellulose, cellulose, and lignin. The Random Nucleation and Growth models (M15–M22) best describe the kinetics, with E_a values ranging from 47.7 to 239.8 kJ mol^{-1}.

Thermodynamic analysis confirms that pyrolysis is endothermic ($\Delta H > 0$) and non-spontaneous ($\Delta G > 0$), necessitating continuous energy input. These findings underscore the potential of DdwFs as a renewable biofuel source, providing valuable insights into the energy requirements and reaction mechanisms crucial for optimizing biomass conversion. This research offers a pathway for improving reactor designs and advancing sustainable biofuel production, contributing to the transition from fossil fuels to eco-friendly energy solutions.

Introduction

Fossil fuels require strict regulation due to their limited reserves and significant environmental impact, particularly their contribution to global warming. Consequently, increasing emphasis is placed on developing reactor designs and processes for converting lignocellulosic biomass waste into renewable energy. Biomass waste is a promising renewable energy source, but its high oxygen and moisture content result in low energy density. To fully realize its potential, biomass is typically upgraded into higher-quality fuels [1,2].

The demand for renewable and eco-friendly biomass has intensified due to fossil fuel depletion and environmental concerns [1–3]. One promising sustainable resource is the biomass fiber of Dracaena draco, a palm species with considerable global availability. Valorizing Dracaena draco waste fibers (DdwFs) for bioenergy production can reduce environmental pollution and dependence on non-renewable fossil fuels. Combustion, a well-established thermochemical process, is commonly used to produce volatiles, charcoal, and bio-oil from biomass [4].

A technique for characterizing the combustion and pyrolysis behavior of solid biomass fibers is Thermogravimetric Analysis (TGA). By adjusting temperature and heating rate, TGA provides valuable

* Correspondence author.
** Correspondence author at: Department of Chemical and Petroleum Engineering, College of Engineering, United Arab Emirates University, PO Box 15551, Al Ain, United Arab Emirates.
E-mail addresses: a.belaadi@univ-skikda.dz (A. Belaadi), jawaid@uaeu.ac.ae (M. Jawaid).

https://doi.org/10.1016/j.ecmx.2025.101494
Received 9 April 2025; Received in revised form 11 October 2025; Accepted 22 December 2025
Available online 23 December 2025
2590-1745/© 2025 The Authors. Published by Elsevier Ltd. This is an open access article under the CC BY license (http://creativecommons.org/licenses/by/4.0/).

Nomenclature

Symbol	Definition
A	Pre-exponential factor (min^{-1})
ARN	Assumed Random Nucleation
CRM	Coats–Redfern method
DdwFs	*Dracaena draco* waste fibers
DTG	Derivative thermogravimetric analysis
dα/dT	Conversion rate with respect to temperature (°C/min)
E_a	Activation energy (kJ/mol)
EGM	Ensuing Growth Model
f(α)	Differential form of conversion function
g(α)	Integral form of conversion function
H	Planck's constant ($6.626 \times 10^{-3} \times J \times s$)
k(T)	Global reaction rate constant
KB	Boltzmann's constant ($1.381 \times 10^{-23} \times J \times K^1$)
KCE	Kinetic compensation effect
lnA	Natural logarithm of pre-exponential factor
m0	Initial mass of sample (g)
Mf	Final residual mass (g)
Mi	Mass at time *t* during pyrolysis (g)
ML	Mass loss (%)
R	Universal gas constant (8.314 J/mol × K)
R^2	Coefficient of determination
RM	Reaction model
TGA	Thermogravimetric analysis
Tiso	Isokinetic temperature (K)
Tp	Peak temperature (K)
A	Conversion degree
B	Heating rate (°C/min)
ΔG	Gibbs free energy change (kJ/mol)
ΔH	Enthalpy change (kJ/mol)
ΔS	Entropy change (kJ/mol × K)

insight into conversion kinetics. It supports both model-free methods (e.g., Kissinger–Akahira–Sunose, Flynn–Wall–Ozawa) [5,6] and model-fitting approaches such as the Coats–Redfern method (CRM) [7]. These methods yield the kinetic triplet parameters: activation energy (E_a), pre-exponential factor (A), and reaction mechanism (RM), from which thermodynamic parameters (ΔH°, ΔG°, ΔS°) can be derived to assess feasibility and energy profiles [8]. Such evaluations are critical for biomass valorization, including DdwFs [9,10]. However, comparisons across studies are often difficult due to variations in experimental conditions, methodologies, and heating rates (β) [11,12].

For instance, Lalaymia et al. investigated the pyrolysis kinetics of Agave americana flower stalk waste (FSSAW) using non-isothermal TGA at β of 30, 40, and 50 °C/min. Kinetic parameters were determined via the Coats–Redfern method across 36 solid-state models, with activation energies ranging from 4.22 to 252.73 kJ/mol. The results confirmed both complex and simple mechanisms, consistent with the kinetic compensation effect. Thermodynamic analysis revealed ΔH values up to 249.65 kJ/mol and ΔG values up to 390.81 kJ/mol, with negative ΔS values indicating a more ordered activated state. Validation by Criado's master plot identified random nucleation and growth (M16) as the dominant mechanism at early decomposition stages [13]. Similarly, Ferfari et al. analyzed the decomposition of Syagrus romanzoffiana rachis fibers (SrWRFs) under nitrogen at β of 30–50 °C/min. Using the Coats–Redfern method and a three-parallel Gaussian model, they resolved hemicellulose, cellulose, and lignin degradation, with activation energies of 97.31–262.11 kJ/mol depending on heating rate. Thermodynamic analysis showed that SrWRF pyrolysis is endothermic ($\Delta H > 0$), non-spontaneous ($\Delta G > 0$), and associated with negative ΔS values, again confirming greater molecular order in the activated complex. The strong lnA–E_a correlation supported the kinetic compensation effect [14].

Similarly, Upee and Zaini [15] conducted an extensive study on biomass pyrolysis, focusing on materials such as cardboard, bamboo, coconut shells, empty fruit bunches, and palm oil. They found that each biomass subgroup followed a distinct reaction mechanism (RM). The typical activation energy (E_a) values varied widely: from 10 to 64 kJ/mol for empty fruit bunches, 8 to 70 kJ/mol for bamboo, 13 to 277 kJ/mol for cardboard, and 18 to 186 kJ/mol for coconut shells. Their findings emphasized that biomass decomposition is an endothermic process that requires external energy to initiate [16]. These studies underscore the significant impact of heating rate (β) on activation energy (E_a) and the importance of selecting appropriate models for accurate kinetic predictions. The comparison of pyrolysis behavior across different lignocellulosic biomasses suggests that similar analyses of *Dracaena draco* waste fibers (DdwFs) could provide valuable insights into their reaction pathways and energy requirements, further advancing our understanding of biomass pyrolysis.

The present study aims to investigate, for the first time, the pyrolysis kinetics and thermodynamics of *Dracaena draco* biomass fibers (DdwFs) to assess their suitability for renewable biofuel applications. The specific objectives of this research are: (i) to determine the kinetic triplet parameters (E_a, A, RM) using the Coats–Redfern method; (ii) to validate kinetic models using Criado's master plot; (iii) to evaluate thermodynamic parameters (ΔH, ΔG, ΔS) to assess energy requirements and process feasibility; and (iv) to correlate kinetic and thermodynamic results with the compositional features of DdwFs, providing insights for reactor optimization and sustainable energy production.

Materials and methods

Preparation of Dracaena draco waste fibers (DdwFs)

*Ddw*Fs were collected from palm trees in the Botanical Garden at the University of Skikda, Algeria. The process begins by peeling and splitting the rachis lengthwise to extract the fibers. The rachis is soaked in water for 40 to 50 days at temperatures ranging from 35 °C to 45 °C. This water-retting process [17] encourages anaerobic bacterial activity, which naturally decomposes the rachis and facilitates fiber extraction. After retting, the fibers are separated by hand, cleaned, and allowed to air dry (Fig. 1) [18].

In addition to fiber preparation, a detailed compositional characterization of Dracaena draco waste fibers (DdwFs) was conducted to support the interpretation of their pyrolysis behavior. Proximate analysis (moisture, volatile matter, fixed carbon, and ash) was performed following ASTM standards. Ultimate analysis was carried out using an elemental analyzer to determine C, H, N, and S contents, with oxygen calculated by difference. The lignocellulosic fractions (cellulose, hemicellulose, and lignin) were quantified using standard chemical procedures based on the Van Soest method.

Thermogravimetric analysis (TGA) and decomposition of Dracaena draco waste fibers (DdwFs): An experimental approach

The decomposition behavior of *Ddw*Fs during pyrolysis was analyzed using a Perkin-Elmer thermogravimetric analyzer [16]. For each test, approximately 6 mg of the material was put in a crucible of alumina and warmed at three different rates (i.e., 15, 25, and 30 °C/min) from 20 °C until 800 °C while being fed with 100 mL/min of nitrogen. The the Coats–Redfern method (CRM) was used to precisely evaluate the kinetic and thermodynamic characteristics derived from the collected

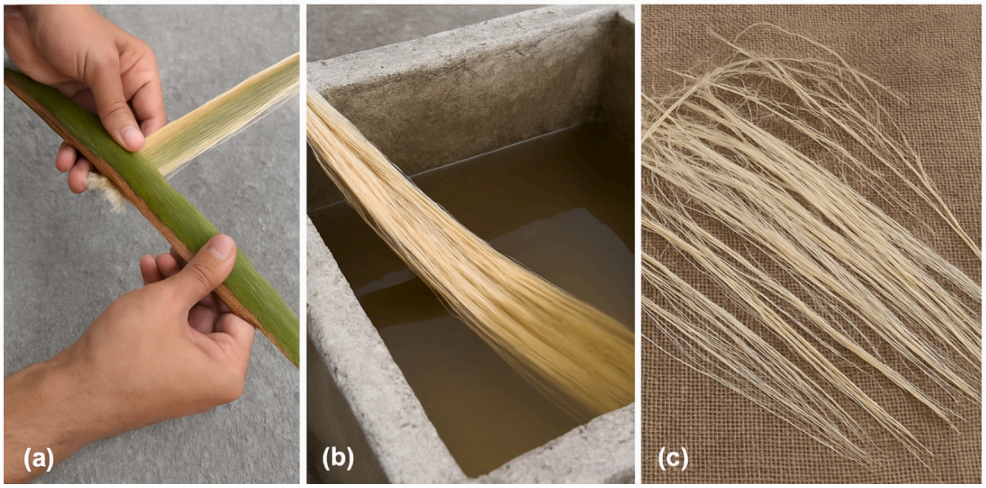

Fig. 1. Extraction process of *Dracaena draco* **biomass fiber** (DdwFs): (a) peeling and splitting of rachis, (b) retting in water, and (c) drying and cleaning of fibers prior to TGA analysis.

thermogravimetric (TG) data.

All thermogravimetric analyses (TGA) were performed in triplicate under identical conditions to ensure reproducibility. The reported results represent the mean values of three runs, and standard deviations were calculated where relevant. The consistency of the data was further confirmed by high determination coefficients ($R^2 > 0.99$) obtained across the applied kinetic models.

Pyrolysis kinetic study

The overall pyrolysis reaction mechanism for *Ddw*Fs (**Equation (1)**) can be described by combining several individual reactions and modeling them as a unified first-order or *n*-order process [19]:

$$DdFs_{(s)} \xrightarrow{k(T)} Volatiles_{(g)} + Biochar_{(s)} \quad (1)$$

k (T) denotes the constant global reaction rate, expressed as follows in **Equation (2)** [20]:

$$k(T) = Ae^{-\frac{E_a}{RT}} \quad (2)$$

The thermal degradation of a sample in the solid state is described by the basic velocity equation in isothermal conditions. The pyrolysis kinetic analysis of *Ddw*Fs was conducted based on the Arrhenius law [21].

$$\frac{d\alpha}{dt} = k(T)f(\alpha) \quad (3)$$

where:

$$\alpha = \frac{m_0 - m_i}{m_0 - m_f} \quad (4)$$

At a constant β:

$$\beta = \frac{dT}{dt} \quad (5)$$

A (min^{-1}) represents the pre-exponential variable, R (8.314 J/mol × K) signifies the universal constant of gas, and E_a (kJ/mol) is the activating energy. The reaction's absolute temperature is indicated by T (K), the starting mass of *Ddw*Fs used in TGA is represented by *m0* (g), the amount of mass remaining at time t during pyrolysis is represented by m_i (g), and the resulting residual quantity is indicated by m_f (g).

Integrating **Equations (3) and (4)** produces the expression found in **Equation (6)** [22].

$$\frac{d\alpha}{dt} = Ae^{-\frac{E_a}{RT}}f(\alpha) \quad (6)$$

In the dynamic TGA experiment, β is represented according to **Equation (7)** [3]:

$$\beta = \frac{dT}{dt} = \frac{dT}{d\alpha} \times \frac{d\alpha}{dt} \quad (7)$$

Equation (8) illustrates how **Equations (6) and (7)** can be integrated to create the non-isothermal speed law [23]:

$$\frac{d\alpha}{dt} = \frac{A}{\beta}e^{-\frac{E_a}{RT}}f(\alpha) \quad (8)$$

Rearranging and incorporating **Equation (8)** yields the conversion function's integral form, $g(\alpha)$, illustrated in **Equation (9)** [24]:

$$g(\alpha) = \int_0^{\alpha} \frac{d\alpha}{f(\alpha)} = \frac{A}{\beta}\int_{T_0}^{T} e^{-\frac{E_a}{RT}}dT \quad (9)$$

Different approximation methods are utilized, with $g(\alpha)$ standing for the RM's integral form, as there is no analytical answer for **Equation (9)**.

Model fit

The kinetic model $f(\alpha)$ is crucial for understanding the dynamics and mechanisms of pyrolytic breakdown. It can be determined through model-fitting techniques like Criado's master plot method and the CRM.

Coats–Redfern method (CRM)

The CRM is often utilized to ascertain kinetic factors, as the sample's (E_a) and A [25]. **Equation (10)** represents the fundamental expression of the CRM used to calculate these kinetic parameters.

$$\ln\left[\frac{g(\alpha)}{T^2}\right] = ln\frac{AR}{\beta E_a}\left(1 - \frac{2RT}{E_a}\right) - \frac{E_a}{RT} \quad (10)$$

Table 1 shows the kinetic equation for various response mechanisms represented by $g(\alpha)$. Drawing $\ln[g(\alpha)/T^2]$ as a function of $1/T$, the resulting linear slope can be used to determine (E_a), while the intercept provides A. Although the response process may affect the precise shape of $g(\alpha)$, most solid-state reactions are classified into one of the thirty-six groups listed in Table 1.

Estimation of the reaction mechanism. 'The master plot demonstrates Criado's reduced master plot method (**Equation (11)**), which forecasts

Table 1
Standard solid-state pyrolysis process models or mechanisms [44–46]. (ARN: Assumed Random Nucleation, 3D: Three-Dimensional Diffusion, 2D: Two-Dimensional, 1D: One-Dimensional).

Model No.	$g(\alpha)$	$f(\alpha)$	Rate-determining reaction mechanism
Non-invoking equations for chemical processes or mechanisms			
M1	$1-(1-\alpha)^{2/3}$	$3/2(1-\alpha)^{1/3}$	Chemical reaction
M2	$1-(1-\alpha)^{1/4}$	$4(1-\alpha)^{3/4}$	
M3	$(1-\alpha)^{-1/2}-1$	$2(1-\alpha)^{3/2}$	
M4	$(1-\alpha)^{-1}-1$	$(1-\alpha)^{2}$	
M5	$(1-\alpha)^{-2}-1$	$1/2(1-\alpha)^{3}$	
M6	$(1-\alpha)^{-3}-1$	$1/3(1-\alpha)^{4}$	
M7	$1-(1-\alpha)^{2}$	$1/2(1-\alpha)$	
M8	$1-(1-\alpha)^{3}$	$1/3(1-\alpha)^{2}$	
M9	$1-(1-\alpha)^{4}$	$1/4(1-\alpha)^{3}$	
Equations for acceleration rates			
M10	$\alpha^{3/2}$	$2/3\alpha^{-1/2}$	Nucleation
M11	$\alpha^{1/2}$	$2\alpha^{1/2}$	
M12	$\alpha^{1/3}$	$3\alpha^{2/3}$	
M13	$\alpha^{1/4}$	$4\alpha^{3/4}$	
M14	$\ln\alpha$	α	
Sigmoidal rate equations or random nucleation and subsequent growth			
M15	$-\ln(1-\alpha)$	$1-\alpha$	ARN and its subsequent growth
M16	$[-\ln(1-\alpha)]^{2/3}$	$3/2(1-\alpha)[-\ln(1-\alpha)]^{1/3}$	
M17	$[-\ln(1-\alpha)]^{1/2}$	$2(1-\alpha)[-\ln(1-\alpha)]^{1/2}$	
M18	$[-\ln(1-\alpha)]^{1/3}$	$3(1-\alpha)[-\ln(1-\alpha)]^{2/3}$	
M19	$[-\ln(1-\alpha)]^{1/4}$	$4(1-\alpha)[-\ln(1-\alpha)]^{3/4}$	
M20	$[-\ln(1-\alpha)]^{2}$	$1/2(1-\alpha)[-\ln(1-\alpha)]^{-1}$	
M21	$[-\ln(1-\alpha)]^{3}$	$1/3(1-\alpha)[-\ln(1-\alpha)]^{-2}$	
M22	$[-\ln(1-\alpha)]^{4}$	$1/4(1-\alpha)[-\ln(1-\alpha)]^{-3}$	
M23	$\ln\alpha/(1-\alpha)$	$\alpha/(1-\alpha)$	Branching nuclei
Equations for decelerating rates Reaction at the phase boundary			
M24	α	1	Contracting disk
M25	$1-(1-\alpha)^{1/2}$	$2(1-\alpha)^{1/2}$	Contracting cylinder (cylindrical symmetry)
M26	$1-(1-\alpha)^{1/3}$	$3(1-\alpha)^{2/3}$	Contracting sphere (spherical symmetry)
The diffusion mechanism based on			
M27	α^{2}	$1/2\alpha$	1D diffusion
M28	$[1-(1-\alpha)^{1/2}]^{1/2}$	$4\left\{(1-\alpha)[1-(1-\alpha)]^{1/2}\right\}^{1/2}$	2D diffusion
M29	$\alpha+(1-\alpha)\ln(1-\alpha)$	$[-\ln(1-\alpha)]^{-1}$	2D diffusion
M30	$[1-(1-\alpha)^{1/3}]^{2}$	$(3/2)(1-\alpha)^{2/3}[1-(1-\alpha)^{1/3}]^{-1}$	3D, spherical symmetry
M31	$1-2/3\alpha-(1-\alpha)^{2/3}$	$(3/2)[(1-\alpha)^{-1/3}-1]^{-1}$	3D, cylindrical symmetry
M32	$[(1-\alpha)^{-1/3}-1]^{2}$	$(3/2)(1-\alpha)^{4/3}[(1-\alpha)^{-1/3}-1]^{-1}$	3D
M33	$[(1+\alpha)^{1/3}-1]^{2}$	$(3/2)(1+\alpha)^{2/3}[(1+\alpha)^{1/3}-1]^{-1}$	
M34	$1+2/3\alpha-(1+\alpha)^{2/3}$	$(3/2)[(1+\alpha)^{-1/3}-1]^{-1}$	
M35	$[(1+\alpha)^{-1/3}-1]^{2}$	$(3/2)(1+\alpha)^{4/3}[(1+\alpha)^{-1/3}-1]^{-1}$	
M36	$[1-(1-\alpha)^{1/3}]^{1/2}$	$6(1-\alpha)^{2/3}[1-(1-\alpha)^{1/3}]^{1/2}$	

the solid-status reaction of pyrolysis process. This method employs a direct model-fitting approach to identify the kinetic mechanism.

$$\frac{Z(\alpha)}{Z(0.5)}=\frac{f(\alpha)\times g(\alpha)}{f(0.5)\times g(0.5)}=\left(\frac{T_{\alpha}}{T_{0.5}}\right)^{2}\frac{\left(\frac{d\alpha}{dt}\right)_{\alpha}}{\left(\frac{d\alpha}{dt}\right)_{0.5}} \tag{11}$$

$T_{0.5}$ and $(d\alpha/dt)_{0.5}$ are the temperature and conversion rate for $\alpha = 0.5$.

The left side of **Equation (11)** shows each reaction mechanism by a reduced theoretical curve, expressed as $\frac{f(\alpha)g(\alpha)}{f(0.5)g(0.5)}$. The right-side **Equation (11)** relates to the lower rate and can determine the experiment's outcome. The reaction process dictates how $f(\alpha)$ is formulated for a specific solid-state response (Table 1).

Estimation of thermodynamic factors

The physical quantities, including enthalpy (ΔH, kJ/mol, **Equation (12)**), Gibb's free energy (ΔG, kJ/mol, **Equation (13)**), and entropy (ΔS, kJ/mol × K, **Equation (14)**), are related to internal energy, thermodynamic potential, and disorder, respectively. These parameters are closely associated with kinetic characteristics and act as indicators of thermal stability [26–28]. To fully understand the thermal decomposition process, it is essential to identify key thermodynamic variables (ΔH, ΔG, and ΔS) [29].

$$\Delta H = E - RT \tag{12}$$

$$\Delta G = Ea + R.T_{m}.\ln\left(\frac{K_B T_m}{h.A}\right) \tag{13}$$

$$\Delta S = \frac{\Delta H^{\circ} - \Delta G^{\circ}}{T_P} \tag{14}$$

$$A^{*} = \left[\beta.E_{a}.\exp\left(\frac{Ea}{RT_m}\right)\right]/(R\ T_m^2) \tag{15}$$

where K_B denotes Boltzmann's value (1.381×10^{-23} J × K^{-1}), h for the constant of Planck (6.626×10^{-34} J × s), and T_p for the derivative thermogravimetric (DTG) curve's peak temperature (K), respectively.

Results and discussion

Thermal decomposition behavior of Dracaena draco waste fibers (DdwFs)

Fig. 2 illustrates the TGA and DTG characteristics of *Ddw*Fs

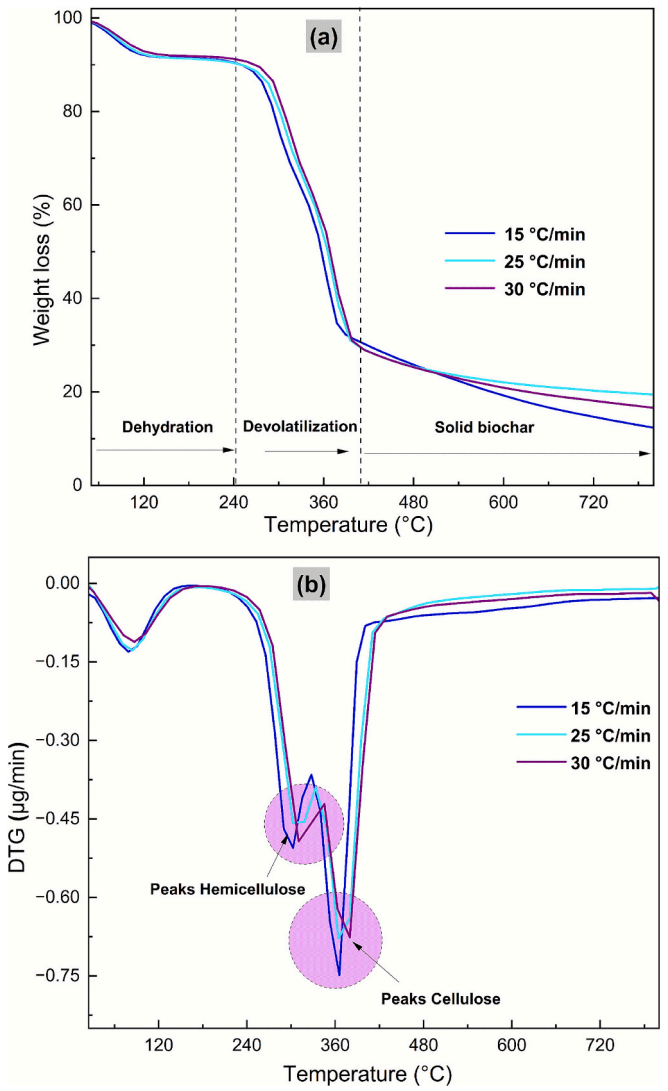

Fig. 2. TGA profiles of the three samples at various heating rates (β): (a) TGA analysis and (b) DTG curves.

decomposition at 15, 25, and 30 degrees Celsius per minute, three distinct β values. The TGA and DTG curves exhibited similar trends across the range of β. As β increased, higher temperatures caused the TGA and DTG curves to change, indicating a delay in the rates of thermal decomposition. This delay is likely due to slower mass and heat transfer processes at higher β values. Notably, when β rose from 15 to 30 °C/min, the *DdwFs* showed signs of temperature hysteresis. This phenomenon was observed as a shift in the TGA curve's mass loss (ML) fraction toward higher temperatures while maintaining consistent thermal decomposition characteristics. Furthermore, the DTG curves revealed broader temperature ranges and slower reaction rates at elevated β, suggesting that the internal temperatures of the samples required more time to reach the breakdown threshold [30].

Table 2
Fibers of *Dracaena draco* waste (*DdwFs*) were examined using thermogravimetric analysis (TGA) and derivative thermogravimetric (DTG) techniques at heating rates (β) of 15, 25, and 30 °C/min (ML: Mass loss).

β (°C/min)	Weight of specimen (mg)	T_i(°C)	T_f(°C)	T_m(°C)	*ML*(%)
15	6.0330	209	415	363	58.96
25	5.0900	226	437	370	61.89
30	5.1970	248	447	380	63.06

Table 2 shows the average pyrolysis temperature, ML percentage, and TGA-DTG data at 15, 25, and 30 °C/min heating rates. As degradation continued, a significant temperature rise was observed. However, there was no noticeable change in ML or volatile emissions during the active pyrolysis phase. During pyrolysis, the ML varied from 59 % to 63.1 % for all three β values (15, 25, and 30 °C/min). The breakdown of thermally stable components was shown by the DTG curve. at lower temperatures, accompanied by several decomposition processes within the active pyrolysis zone [31].

At heating rates of 15, 25, and 30 °C/min, the total mass loss of DdwFs ranged between 59 % and 63.1 %. Hemicellulose decomposition occurred between 140–290 °C, cellulose between 290–400 °C, and lignin between 400–800 °C, consistent with the measured lignocellulosic fractions (26.7 %, 38.5 %, and 31.4 %, respectively).

The decomposition stages of DdwFs align with those reported for other lignocellulosic biomasses, confirming the general consistency of pyrolysis pathways. Hemicellulose degraded between 140–290 °C, cellulose between 290–400 °C, and lignin above 400 °C. These intervals are comparable to the decomposition ranges of *Agave americana* fibers (150–400 °C) [13] and *Syagrus romanzoffiana* fibers (200–650 °C) [14], highlighting that while the fundamental mechanisms are similar, the specific ranges for DdwFs indicate relatively higher stability of the lignin fraction. Such stability is beneficial for char production, suggesting potential applications of DdwFs in carbon-rich biochar generation.

Consistent with previous studies, biomass decomposition proceeded through distinct thermal stages [32]. After the initial moisture evaporation (room temperature to ~ 140 °C), hemicellulose decomposed between 140–290 °C, cellulose between 290–400 °C, and lignin over a broader range of 400–800 °C, reflecting its more complex, multi-step degradation behavior. The reported values represent averages from three replicate experiments, with only minor deviations, confirming the reproducibility of the results.

The DTG peaks correspond closely with the measured lignocellulosic composition of DdwFs (Table 3), supporting the assignment of hemicellulose, cellulose, and lignin decomposition stages. These findings align with results reported for other lignocellulosic biomasses. For example, in Energy Conversion and Management, the co-pyrolysis of Rosa rubiginosa rosehip seed and husk wastes demonstrated that compositional factors strongly influence kinetic parameters and product distribution, with lignin content in particular contributing to char yield and thermal stability [32,33]. This comparison highlights the value of proximate, ultimate, and lignocellulosic characterization (Table 3) in contextualizing the degradation stages of DdwFs and validating the observed decomposition behavior.

Table 3
Compositional characterization of *Dracaena draco* waste fibers (DdwFs).

Parameter	Value (wt%)
Proximate analysis	
Moisture content	7.8
Volatile matter	71.2
Fixed carbon	17.5
Ash content	3.5
Ultimate analysis (dry basis)	
Carbon (C)	46.8
Hydrogen (H)	6.3
Nitrogen (N)	0.9
Sulfur (S)	0.2
Oxygen (O, by difference)	45.8
Lignocellulosic composition	
Cellulose	38.5
Hemicellulose	26.7
Lignin	31.4

Kinetic analysis

Fig. 3 displays the variations in transformation level (α) as well as its derivative (dα/dT) for β *vs* temperature (T) during 15, 25, and 30 °C/min. Table 4 provides the mean values of dα/dT over the pyrolysis duration, the maximum dα/dT, and the corresponding temperature at which it occurs. It was noted that most of the *DdwFs*' pyrolysis took place between 120 and 550 °C.

As β increased, both α and dα/dT shifted to higher temperature ranges, displaying only slight changes in the shapes of the curves. Temperature hysteresis arises when a sample's thermal transfer rate does not align with the external β, leading to a lag between the material's actual and programmed temperatures. This phenomenon occurs because heat requires time to propagate through the sample, especially in materials with low thermal conductivity or complex structures.

As a result, during heating or cooling cycles, the sample's temperature differs from that of the surrounding environment, causing variations in thermal events such as phase transitions or decomposition. This phenomenon is often observed in thermal analysis techniques like TGA, where rapid heating can cause variations in recorded temperatures due to delayed heat absorption or release.

As β increased, hysteresis effects became more pronounced, but the maximum and average dα/dT values remained nearly unchanged. The inverse relationship between the dα/dT ratio and β likely explains this observation. As β increases, the temperature at which maximum dα/dT occurs also rises, canceling the opposing effects of T and β on dα/dT (see Fig. 3).

For the kinetic analysis of *DdwFs*, ln$A$ and (E_a) were determined using the CRM. Table 5 displays the results, including ln$A$, R^2, and (E_a) for various kinetic models at different β values. The chemical models that demonstrated a good fit (i.e., $R^2 > 0.99$) included sigmoidal rate equations for random nucleation followed by growth and declaratory rate equations for β values of 15, 25, and 30 °C/min. At 15 °C/min, the favorable models (M2, M15, M20, M21, M22, M30, and M32) exhibited good R^2 values. At a rate of 25 °C/min, models M1, M2, M15, M20, M21, M22, M25, M26, M30, and M32 also showed excellent fits, with M15, M20, M21, M22, and M32 having the highest R^2 values. Other models displayed inadequate fits with lower R^2 values.

The kinetics evaluation concentrated upon the productive pyrolysis zone, thereby is typically thought of as a single-step procedure. Based on the heat degradation behavior, several kinetic models were proposed to describe DdwFs pyrolysis [30]. Table 5 presents the thirty-six solid-state

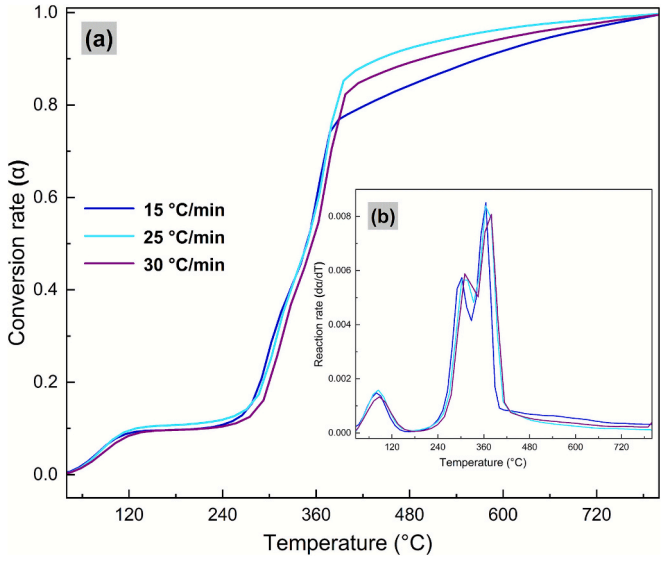

Fig. 3. Variations in the conversion rate (α) and its derivative (dα/dT) as a function of temperature (T).

Table 4
Corresponding temperature (T) along with the maximum and average values of dα/dT. (β: Heating rate).

β(°C/min)	Maximum $\frac{d\alpha}{dT}$ (T^{-1})/T (°C)	Average $\frac{d\alpha}{dT}$ (T^{-1})
15	8.5×10^{-3}/368.69	1.22×10^{-3}
25	8.2×10^{-3}/366.84	1.18×10^{-3}
30	7.9×10^{-3}/383.26	1.18×10^{-3}

RMs, categorized into four groups of response mechanisms, as well as each model's corresponding kinetic settings (E_a and ln$A$). Table 5 also shows the TGA results using various solid-state kinetic model functions for β values of 15, 25, and 30 °C/min. The correlation coefficient (R^2) values demonstrate a good fit for all the kinetic models.

Fig. 4 illustrates how (E_a) and the regression values in the TGA findings correlate with each other. Models M15, M20, M21, M22, and M30, all with R^2 values exceeding 0.99, were the most suitable diffusivity models. Fig. 5 illustrates the optimal models for region I at β values of 15, 25, and 30 °C/min. The kinetic parameters for various types of biomasses are summarized in Table 5, as determined by the CRM. For all β values, the models exhibiting the highest R^2 values (i.e., $R^2 > 0.99$) were the equations with sigmoidal rates or those representing probability nucleation followed by subsequent growth (M15, M20, M21, and M22).

The (E_a) values calculated for these models were as follows: for M15, 47.74, 51.43, and 52.32 kJ/mol at a β of 15, 25, and 30 °C/min, respectively. For M20, the (E_a) values were 105.40, 112.86, and 114.8 kJ/mol. For M21, the (E_a) values were 163.06, 174.31, and 177.3 kJ/mol, respectively. For M22, the (E_a) values were 220.73, 235.75, and 239.8 kJ/mol (Fig. 5**(a-c)**). Based on the optimal adaptation of M15, M20, M21, and M22, the average E_a for *DdwFs* varied from 134.23 to 146.05 kJ/mol.

The best-fit models (M15–M22) yielded E_a values of 47.7–239.8 kJ/mol, depending on β and conversion degree. For instance, at β = 15 °C/min, M15, M20, M21, and M22 exhibited E_a values of 47.7, 105.4, 163.1, and 220.7 kJ/mol, respectively. These quantitative differences confirm the multi-step character of DdwF pyrolysis.

As β increased from 15 to 30 °C/min, the (E_a) values declined across all reaction mechanism models, indicating that β strongly influences the kinetic parameters, particularly Ea and lnA. This correlation reflects both heat and mass transfer effects within the porous biomass structure. At higher β, rapid heating creates temperature gradients inside DdwFs particles, leading to incomplete internal heat transfer and localized thermal lag. At the same time, mass transfer resistance can trap volatile products within the fiber matrix, slowing their release and altering the apparent kinetics. These combined effects intra-particle heat conduction and diffusion-controlled volatile escape explain the observed β (E_a) relationship. Similar trends have been reported for other lignocellulosic biomasses, where structural porosity significantly affects apparent kinetic parameters. The data also show that as β increases, (E_a) decreases while lnA rises, consistent with the kinetic compensation effect. Additionally, R^2 values highlight that higher β reduces model fit quality for certain mechanisms, reinforcing the importance of considering heat and mass transfer limitations in kinetic interpretation.

Fig. 6 illustrates the (E_a) values for the pyrolysis of *DdwFs* at various β values of 15, 25, and 30 °C/min, calculated using the RM. (E_a) denotes the energy barrier needed to release volatile compounds during pyrolysis or the energy required to initiate the chemical processes that cause biomass fiber to decompose thermally. The (E_a) profiles varied significantly, underscoring the complex nature of the pyrolysis process [30–34].

Typically, reactions that require higher (E_a) values are slower, taking more time to complete thermal decomposition and occurring at higher temperatures [35]. Although the material's inherent characteristics significantly influence (E_a), all β values showed a substantial rise in (E_a)

Table 5
Thermogravimetric (TG) data at heating rates (β) of 15, 25, and 30 °C/min were used to calculate the activation energy (E_a) and the natural logarithm of the pre-exponential factor (ln$A$) using the Coats-Redfern method (CRM).

No.	15 °C/min			25 °C/min			30 °C/min		
	R^2	ln(A)(min^{-1})	E_a(kJ/mol)	R^2	Ln(A)(min^{-1})	E_a(kJ/mol)	R^2	ln(A)(min^{-1})	E_a(kJ/mol)
M1	0.983	8.68	38.102	0.991	10.2	39.707	0.977	7.31	40.18
M2	0.990	11.05	43.927	0.992	12.26	46.732	0.988	9.39	47.45
M3	0.989	16.04	56.078	0.978	16.5	61.904	0.988	47.59	63.25
M4	0.983	19.89	65.353	0.961	19.69	70.440	0.966	47.46	70.0
M5	0.964	28.7	86.446	0.926	26.87	101.14	0.956	12.73	104.43
M6	0.946	38.75	110.31	0.897	34.99	132.10	0.934	8.54	136.9
M7	0.916	2.91	23.547	0.941	4.86	24.159	0.908	2.56	23.09
M8	0.808	0.04	15.963	0.806	1.97	15.074	0.743	1.06	15.21
M9	0.645	−1.93	10.399	0.625	−0.17	9.386	0.558	0.22	9.60
M10	0.979	13.9	55.819	0.987	16.43	57.166	0.969	38.03	57.75
M11	0.945	0.08	11.989	0.965	0.93	12.378	0.923	0.51	12.45
M12	0.845	−2.22	4.684	0.901	−1.64	4.913	0.796	0.37	4.907
M13	0.303	−3.37	1.031	0.461	−2.93	1.181	0.255	0.73	1.13
M14	–	–	–	–	–	–	–	–	–
M15	0.991	12.61	47.738	0.990	13.6	51.426	0.990	19.97	52.32
M16	0.989	6.13	28.517	0.988	6.8	30.946	0.988	4.1	31.48
M17	0.986	2.89	18.906	0.985	3.39	20.705	0.985	1.69	21.06
M18	0.974	0.35	9.295	0.976	−0.01	10.465	0.974	0.18	10.64
M19	0.939	1.96	4.490	0.953	−1.7	5.3453	0.944	0.38	5.43
M20	0.993	32.05	105.40	0.991	34.03	112.86	0.992	11.85	114.8
M21	0.993	51.48	163.06	0.991	54.45	174.31	0.992	7.72	177.3
M22	0.993	70.92	220.73	0.992	74.87	235.75	0.993	6.56	239.8
M23	–	–	–	–	–	–	–	–	–
M24	0.974	6.99	33.904	0.983	8.68	34.772	0.962	5.65	35.10
M25	0.987	9.59	40.354	0.993	11	42.399	0.983	8.24	42.96
M26	0.989	10.55	42.710	0.993	11.84	45.248	0.987	9.09	45.91
M27	0.981	20.81	77.734	0.988	24.18	79.559	0.972	31.9	80.41
M28	0.975	1.38	15.214	0.987	2.09	16.192	0.969	0.94	16.38
M29	0.987	24.04	85.784	0.993	27.1	88.934	0.982	23.63	90.03
M30	0.991	27.93	95.345	0.994	30.49	100.51	0.989	21.64	102.01
M31	0.989	25.33	88.950	0.994	28.22	92.753	0.985	30.15	93.98
M32	0.992	36.54	116.31	0.985	37.82	126.51	0.991	12.53	129.07
M33	0.974	17.79	69.628	0.983	21.16	70.830	0.964	50.43	71.63
M34	0.977	18.76	72.233	0.985	22.13	73.630	0.967	93.56	74.44
M35	0.966	15.02	62.093	0.97	18.34	62.750	0.954	19.4	63.51
M36	0.981	1.86	16.392	0.989	2.51	17.616	0.977	1.09	17.86

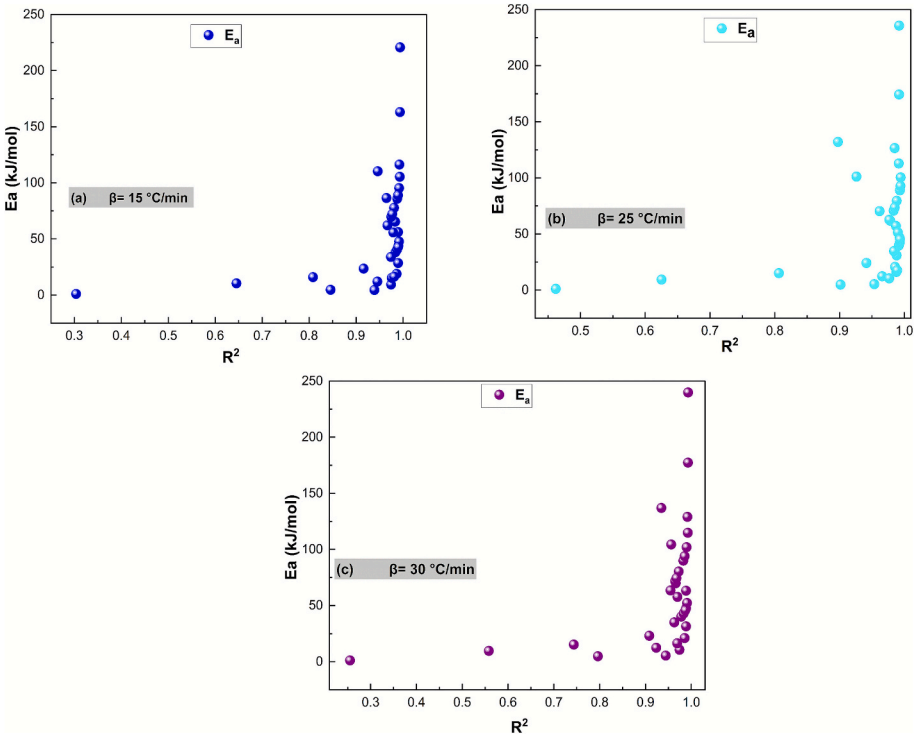

Fig. 4. Activation energy (E_a) *vs.* correlation coefficient (R^2) at various heating rates (β): 15 °C/min, (b) 25 °C/min, and (c) 30 °C/min.

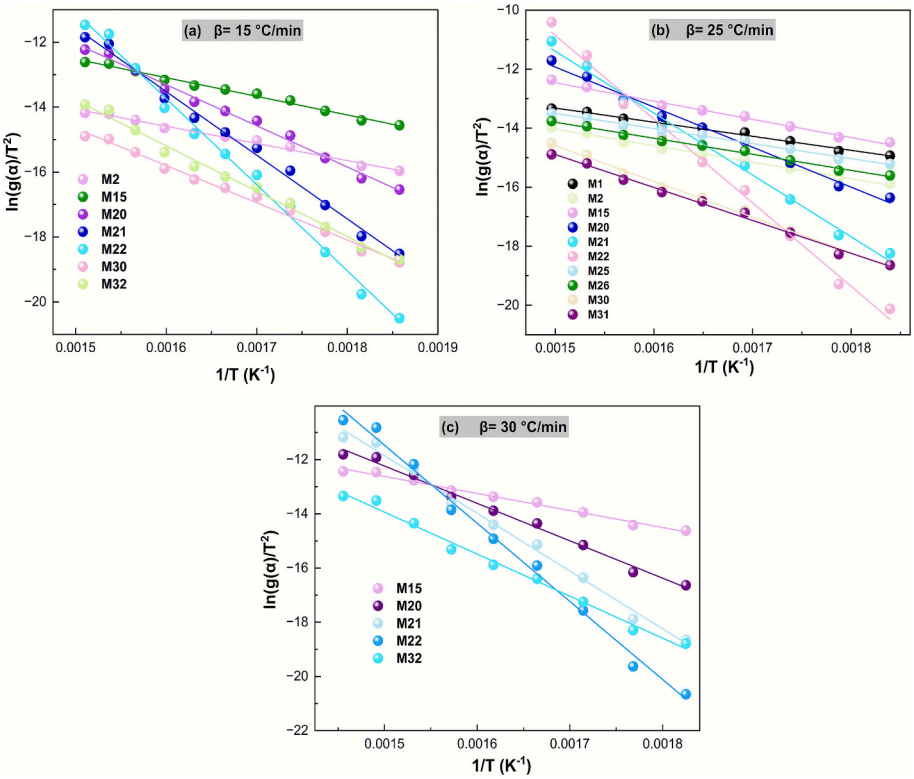

Fig. 5. Fitting patterns of the integral method for estimating the kinetic parameters of *DdwFs* during pyrolysis, using various diffusion and reaction order models at various heating rates (β): (a)15 °C/min, (b) 25 °C/min, and (c) 30 °C/min.

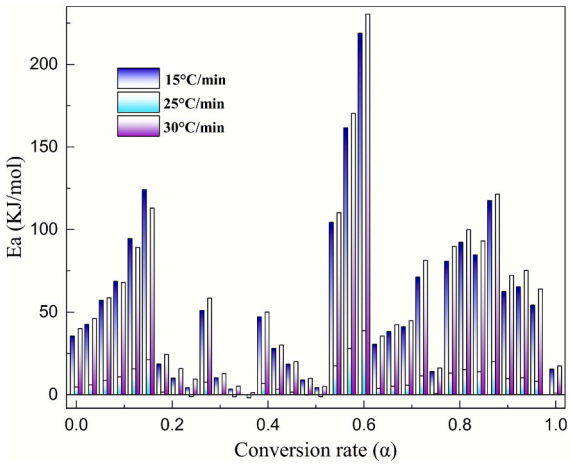

Fig. 6. Activation energy (E_a) *vs.* conversion rate (α).

with higher transformation degrees (i.e., $\alpha > 0.7$) and a gradual increase at lower conversion degrees ($\alpha < 0.4$).

This finding suggests that α significantly influences (E_a). The variation in (E_a) as a function of α can be linked to structural alterations and the heat-driven breakdown process's multistep character [36]. A consistent (E_a) indicates the substance breaks down uniformly in a single-step reaction mechanism. At the same time, significant fluctuations in (E_a) (whether increases or decreases) suggest that the decomposition takes place through several sequential or parallel reactions [37]. At higher conversion levels, the rise in (E_a) can be attributed to the degradation of char due to carbon bonding in polymers, side-chain cyclisation, or polycondensation [38].

The kinetic compensation effect (KCE) describes the correlation established between E_α and $Ln(A)$ [39–41]. This is represented by

Equation (16):

$$\ln A = a + b \times E_\alpha \tag{16}$$

a and b are fixed values derived from experimental kinetic data.

The observed decrease in apparent activation energy (E_a) with increasing heating rate (β) suggests that thermal and mass transfer effects within the porous structure of DdwFs significantly influence the pyrolysis kinetics. At higher β, the external heating creates steep temperature gradients within the biomass fiber particles, leading to incomplete heat penetration and localized thermal lag. This results in delayed decomposition of cellulose and lignin, which artificially elevates the apparent (E_a). Furthermore, volatile products produced during pyrolysis may become temporarily trapped within the fiber matrix at higher β, requiring additional energy for their release. These combined effects resistance to heat conduction and diffusion-limited volatile escape offer a more comprehensive explanation for the (β)-(E_a) correlation, which aligns with similar findings observed in other lignocellulosic biomasses such as *Agave americana*[13] and Syagrus romanzoffiana [14].

Fig. 7 presents ln$A$ as a function of (E_a), derived from the CRM. Table 5 provides detailed information on the KCE parameters, including the values for a, b, K_{iso}, isokinetic temperature (T_{iso}), and R^2. It also describes the decomposition model.

As mentioned earlier, the RM selected for the CRM is considered valid if the calculated T_{iso} falls within the temperature range typical for the pyrolysis process [42]. In this study, the T_{iso} ranges from 120 to 600 °C, corresponding to the temperature interval observed during *Dd*F pyrolysis. The high R^2 values obtained demonstrate a strong fit for the kinetic models, reinforcing their validity. Consequently, thirty-six different types of response models were tested, yielding meaningful results.

The relationship between (E_a) and the natural logarithm of A (i.e., ln$A$) for all β values is expressed as:

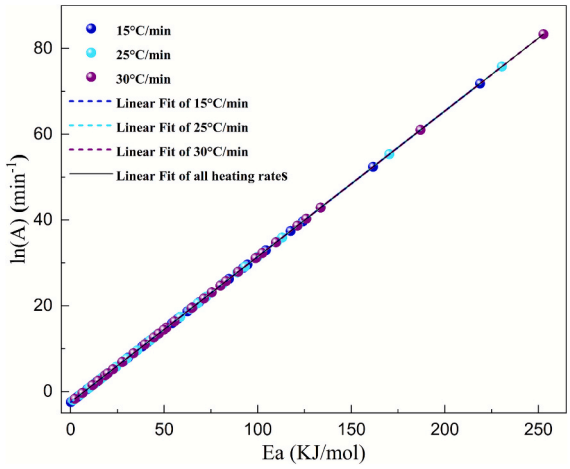

Fig. 7. Isokinetic relationships (ln$A$ *vs.* E_a) at different heating rates (β) using the Coats-Redfern method (CRM).

$$\ln A = -2.4996 + 0.3369 \times E_a \quad (17)$$

Equation (17) further clarifies the relationship between ln$A$ and (E_a), reaffirming the consistent trend observed across various β values.

The calculated activation energies (E_a) for DdwFs, ranging from 47.7 to 239.8 kJ/mol depending on the kinetic model and β, demonstrate the multi-step nature of pyrolysis. These values fall within the typical range reported for lignocellulosic biomasses but show distinct differences compared to other materials. For example, surgical mask waste pyrolysis exhibits an average E_a of 237.2 kJ/mol [46], chicken manure pyrolysis yields 140–151 kJ/mol [43], and jeans waste ranges between 70–148 kJ/mol [44]. This comparison highlights that DdwFs require higher activation energy in certain steps, indicating stronger bonding or structural resistance, especially during lignin decomposition. Such insights underscore the importance of adapting heating strategies when designing pyrolysis reactors for DdwFs.

Kinetic analysis of Criado's master plot compared to the Coats-Redfern method (CRM) for the pyrolysis of Dracaena draco waste fibers (DdwFs)

For each solid-state RM applied to the three β values in this study, models with higher $R2$ values were combined with the experimental data from the TGA using Criado's method, as shown in **Equation (11)**. Table 1 summarizes the corresponding functions of the models, $g(\alpha)$ and $f(\alpha)$. Fig. 8 presents the master curve plots of $g(\alpha)/g(0.5)$ *vs.* α for various mechanistic models based on the approach described by Criado. The rate of ML, derived directly using the DTG curve, is first plotted on the experimental curve.

Further investigation is needed to thoroughly evaluate the best response model for *DdwFs* pyrolysis. Criado's master plot method provides a straightforward and effective fitting technique that relies entirely on experimental data for model assumptions. However, it does not deliver the (E_a) value. It is essential to note that beyond an α of 0.55, the assumed random nucleation (ARN) of the resulting growth (EGM) model may be insufficiently representative of the *Ddw*Fs pyrolysis mechanism. Consequently, the process of pyrolysis could involve a multi-stage response mechanism.

The conclusions drawn in this analysis might not be entirely accurate, as not all kinetic triplets outlined in **Equation (11)** are taken into account. Nevertheless, the assumed random nucleation (ARN) and its ensuing growth model (EGM), considered the primary models for explaining the degradation mechanism of *DdwFs*, are central to both the CRM and Criado's methodologies. These models demonstrate how diffusion becomes the limiting factor in the degradation process of *DdwFs*. The diffusive escape of volatile species governs the rate of solid breakdown. The ARN and (EGM) models further elucidate the cylindrical shape of solid particles and the radial diffusion via a reaction zone that is expanding inside the cylinder-shaped shell, as explained by

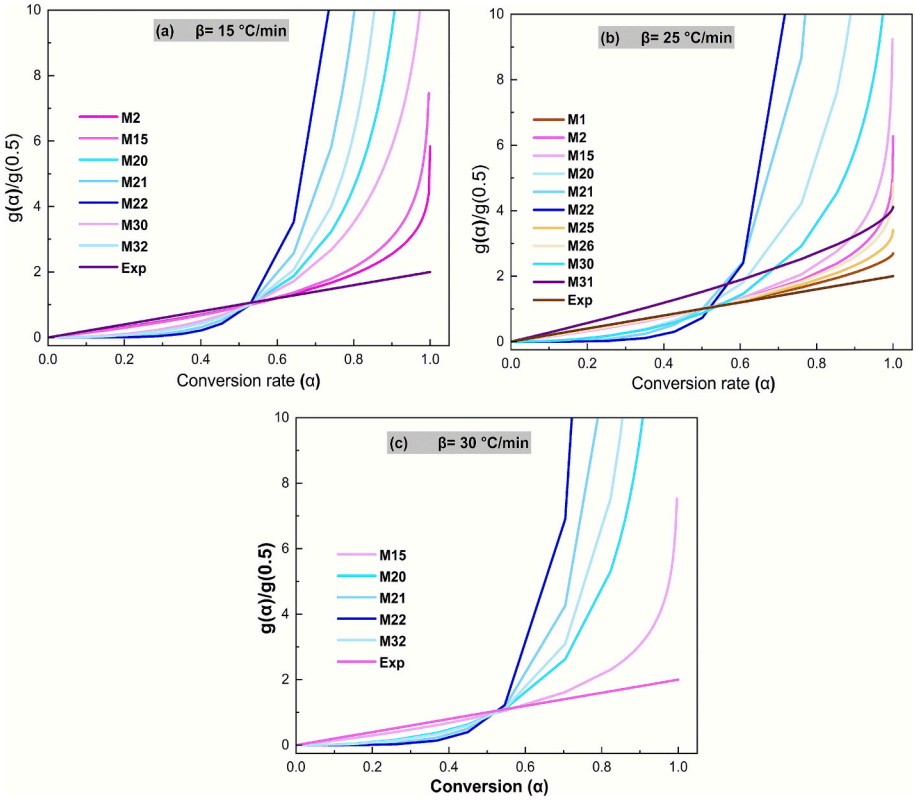

Fig. 8. Criado's master plot for DdwFs at heating rates (β): (a) 15 °C/min, (b) 25 °C/min, and (c) 30 °C/min.

previous studies [45].

Thermodynamic parameter analysis

Fig. 9 and Table 6 display the variations in ΔH, ΔS, and ΔG with α at β of 15, 25, and 30 °C/min. Fig. 9 illustrates that the ΔH values vary from −4.99 to 247.65 kJ/mol, the ΔG values range from 162.61 to 395.81 kJ/mol, and the ΔS values fluctuate between −0.301 and −0.221 kJ/mol·K. On average, ΔH, ΔS, and ΔG values determined by each breakdown technique are 55.17 kJ/mol, −0.243 kJ/mol, and 203.89 kJ/(mol·K), respectively.

Previous studies indicate that ΔH represents the energy difference between reactants and products [46,47]. A positive ΔH value denotes an endothermic process in which reactants have lower energy than products. Since most ΔH values are positive for all α values (Fig. 9a), DdwFs pyrolysis is confirmed as an endothermic process. Moreover, ΔH values show little dependence on β at constant α, suggesting stable heat requirements across heating rates. According to the literature, thermal degradation is feasible when the average difference between (E_a) and ΔH is below 60 kJ/mol [48]. In this study, the difference was ~ 5 kJ/mol, reinforcing the thermal feasibility of DdwFs pyrolysis. The trend of ΔH with α also parallels that of (E_a), further supporting this relationship.

ΔG reflects the spontaneity and feasibility of a reaction [49]. As ΔG increases, the probability of reaction decreases. The consistently positive ΔG values observed (Fig. 9b) indicate that DdwFs pyrolysis is non-spontaneous and requires external energy input, confirming it is a controlled process. In addition, ΔG values rise with both α and β, implying more intensive molecular interactions and faster thermal degradation, though at the cost of reduced spontaneity. This highlights the importance of stable reactor conditions and continuous energy supply for efficient operation.

Entropy (ΔS) represents the degree of disorder in the system [25,50,51]. Negative ΔS values (Fig. 9c), commonly observed at thermal equilibrium [35]. suggest that the activated complex is more ordered than the raw material [37]. This ordering is especially evident in the 200–550 °C active pyrolysis zone identified by the CRM. The negative entropy values point to diffusion-limited behavior, which directly affects gas release during pyrolysis. In practical terms, this implies that slower diffusion rates could restrict conversion efficiency if not properly addressed in reactor scale-up, for example by enhancing mixing or employing designs that mitigate mass transfer limitations.

Overall, ΔG, ΔH, and (E_a) reached their maximum values as β increased from 15 to 30 °C/min, indicating stronger molecular resistance at higher heating rates. The combined kinetic and thermodynamic results thus provide key insights into the energy profile, degree of conversion (α), and reaction mechanism, all of which are essential for bioenergy applications [44]. The positive ΔH values confirm the requirement for continuous heat input, emphasizing the need for optimized heating strategies and possible integration with waste-heat recovery. The consistently positive ΔG values reinforce the non-spontaneous, controlled nature of the process, while negative ΔS values reveal a diffusion-limited system that must be accounted for during reactor design and scale-up. Together, these findings demonstrate that thermodynamic analysis not only characterizes reaction pathways but also delivers practical guidance for improving reactor performance, energy efficiency, and the sustainable integration of DdwFs pyrolysis into biofuel systems.

Across all models, ΔH values varied from –4.99 to 247.65 kJ/mol,

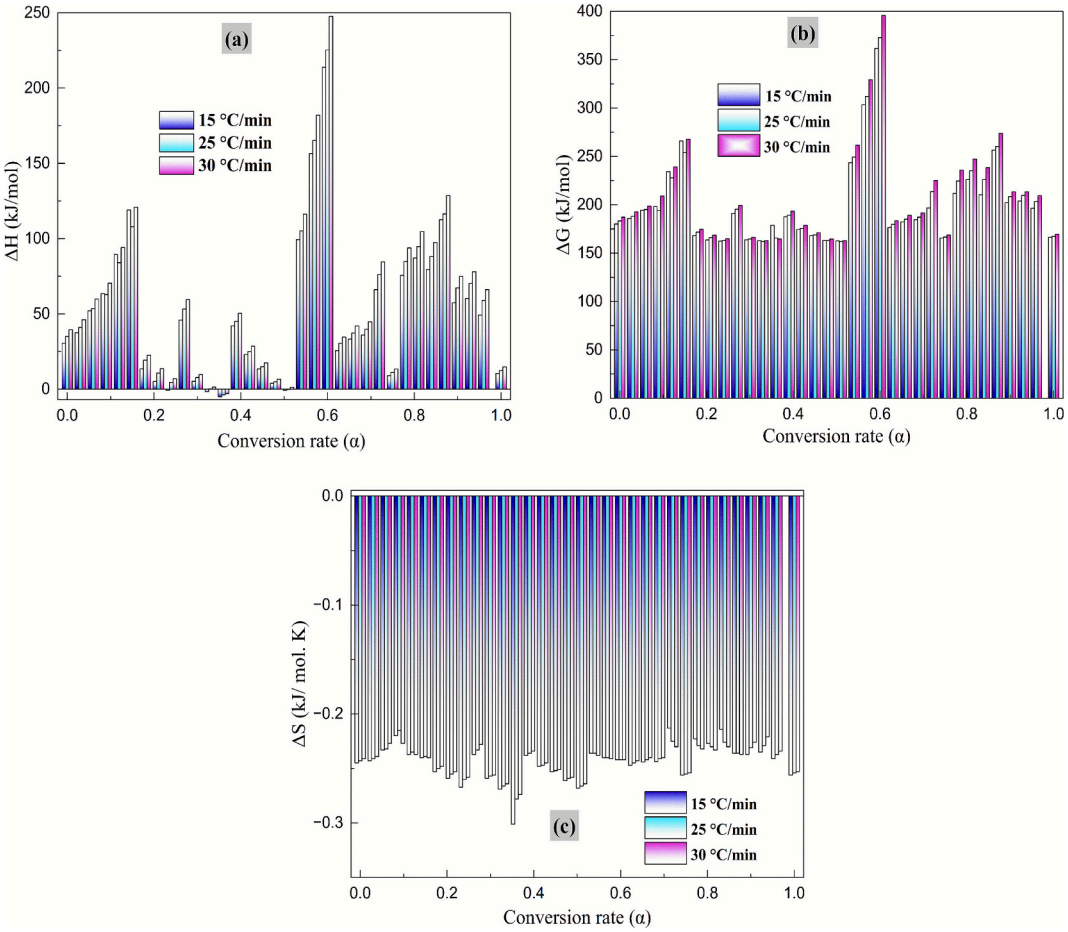

Fig. 9. Variations of thermodynamic parameters ΔH, ΔS, and ΔG *vs* conversion rate (α).

Table 6
Thermodynamic parameters of *Dracaena draco* waste fibers (*DdwFs*). (β: Heating rate).

β (°C/m)	15			25			30		
Model No.	ΔH° kJ/mol	ΔG° kJ/mol	ΔS° kJ/ mol. K	ΔH° kJ/mol	ΔG° kJ/mol	ΔS° kJ/ mol. K	ΔH° kJ/mol	ΔG° kJ/mol	ΔS° kJ/ mol. K
M1	30.506	180.219	−0.245	34.980	183.204	−0.243	39.427	187.103	−0.241
M2	37.476	185.8775	−0.243	41.070	188.277	−0.241	46.097	192.626	−0.239
M3	52.196	194.270	−0.233	53.550	195.0168	−0.232	59.897	198.551	−0.227
M4	63.526	198.171	−0.220	62.930	194.151	−0.215	70.357	209.025	−0.227
M5	89.476	234.295	−0.237	84.070	227.817	−0.235	94.057	239.158	−0.237
M6	119.046	265.925	−0.240	107.980	254.005	−0.239	120.867	267.834	−0.240
M7	13.506	168.198	−0.253	19.270	171.677	−0.250	22.527	174.593	−0.248
M8	5.0661	163.541	−0.259	10.770	166.165	−0.255	13.587	168.540	−0.253
M9	−0.763	162.611	−0.267	4.450	163.014	−0.260	6.987	164.782	−0.258
M10	45.876	190.940	−0.237	53.350	195.364	−0.233	59.537	199.306	−0.228
M11	5.1761	163.706	−0.259	7.700	164.604	−0.257	9.647	166.273	−0.256
M12	−1.6039	162.902	−0.269	0.090	162.221	−0.266	1.337	162.933	−0.264
M13	−4.993	178.923	−0.301	−3.709	165.683	−0.278	−2.822	164.550	−0.274
M14	–	–	–	–	–	–	–	–	–
M15	42.076	187.559	−0.238	45.010	189.301	−0.236	50.447	193.384	−0.234
M16	22.996	174.415	−0.248	24.970	175.535	−0.247	28.537	178.732	−0.245
M17	13.456	168.071	−0.253	14.950	168.748	−0.252	17.577	171.114	−0.251
M18	3.9161	163.100	−0.261	4.930	163.205	−0.259	6.6179	164.597	−0.258
M19	−0.853	162.668	−0.268	−0.089	162.163	−0.266	1.1479	162.840	−0.264
M20	99.316	243.598	−0.236	105.150	249.473	−0.236	116.177	261.617	−0.238
M21	156.556	303.412	−0.240	165.280	311.943	−0.240	181.907	329.335	−0.241
M22	213.796	361.539	−0.242	225.420	372.906	−0.242	247.647	395.810	−0.242
M23	–	–	–	–	–	–	–	–	–
M24	25.526	176.499	−0.247	30.520	179.795	−0.245	34.597	183.421	−0.243
M25	33.196	182.327	−0.244	37.350	185.089	−0.242	42.017	189.148	−0.240
M26	36.016	184.617	−0.243	39.810	187.151	−0.241	44.707	191.386	−0.240
M27	66.226	196.707	−0.213	76.170	213.541	−0.225	84.477	225.117	−0.230
M28	9.0161	165.699	−0.256	11.110	166.602	−0.255	13.367	168.641	−0.254
M29	75.7361	211.911	−0.223	84.750	224.645	−0.229	93.777	235.893	−0.232
M30	87.206	226.019	−0.227	94.730	235.236	−0.230	104.707	247.253	−0.233
M31	79.536	210.442	−0.214	88.060	225.973	−0.226	97.397	238.315	−0.230
M32	112.536	256.682	−0.236	116.330	260.312	−0.236	128.557	273.733	−0.237
M33	57.346	202.099	−0.237	67.250	208.4501	−0.231	74.997	213.362	−0.226
M34	60.196	203.938	−0.235	70.120	209.757	−0.229	78.037	213.303	−0.221
M35	49.166	196.392	−0.241	58.960	203.410	−0.237	66.177	209.254	−0.234
M36	10.426	166.560	−0.256	12.340	167.427	−0.254	14.707	169.582	−0.253

ΔG from 162.61 to 395.81 kJ/mol, and ΔS from –0.301 to –0.221 kJ/mol·K. On average, ΔH was ~ 55 kJ/mol, confirming the endothermic nature of the process, while positive ΔG values confirmed the non-spontaneous character of pyrolysis.

The consistently positive enthalpy values (ΔH) confirm that DdwF pyrolysis is endothermic and requires sustained external heat input. This aligns with the average difference of ~ 5 kJ/mol between E_a and ΔH, indicating a feasible but energy-intensive process. The positive Gibbs free energy values (ΔG) demonstrate that the reactions are non-spontaneous, meaning reactor operation must rely on controlled energy supply, such as coupling with syngas combustion or waste-heat recovery systems. Meanwhile, the negative entropy changes (ΔS) suggest a transition to a more ordered activated state, reflecting diffusion-limited processes where volatile release is constrained. This has direct implications for scale-up: if not accounted for, limited diffusion could reduce gas yields and overall conversion efficiency.

The thermodynamic parameters further emphasize the endothermic and non-spontaneous nature of DdwF pyrolysis. The average enthalpy (ΔH ≈ 55 kJ/mol) is consistent with values reported for other biomass materials, such as rice husk (50–60 kJ/mol) [29] and jeans waste (≈57 kJ/mol) [44]. Similarly, the positive Gibbs free energy values (162–396 kJ/mol) are in line with those observed for Agave americana (up to 390 kJ/mol) [13], confirming the necessity for external energy input across various biomass types. The negative entropy values (–0.301 to –0.221 kJ/mol•K) indicate a transition to a more ordered activated complex, which aligns with the diffusion-limited pyrolysis behavior seen in Syagrus romanzoffiana [14]. These comparisons reinforce the validity of our findings, while the specific thermodynamic ranges of DdwFs highlight its distinctive energy profile. Table 7 further demonstrates that the thermodynamic properties of DdwFs are comparable to those of other biomass materials documented in the literature.

The kinetic and thermodynamic parameters obtained in this study provide practical insights into the application of Dracaena draco waste fibers in thermochemical conversion systems. The predominance of

Table 7
Comparison of kinetic parameters between the current study and previous research. (*DdwFs*: *Dracaena draco* waste fibers, E_a: Activation energy, *A*: Pre-exponential factor, RM: Reaction model, β: Heating rate).

Specimen	β(°C/min)	Average E_a (kJ/mol)	Average *A* (1/min)	RM $g(\alpha)$	Ref
DdwFs	15, 25, 30	218.87 –252.73	7.46 to 7.64	$[-\ln(1-\alpha)]^4$	This study
Surgical face mask	15, 20, 25, 30	237.19	1.36×10^{14}	$[-\ln(1-\alpha)]^{2/3}$	[46]
Agave americana L. fibers	5, 10, 20	83.6—210.1	179.56	$(1-\alpha)^{-1/2}-1$	[26]
Jeans waste	10, 20, 30, 40	70.41 – 148.16	5.5×10^{9} to 1.1×10^{10}	$[1-(1-\alpha)^{1/3}]^2$	[52]
Chicken waste	10, 15, 25	140.4 – 151.2	2.9×10^{9} to 4×10^{10}	$[1/(1-\alpha)]-1$	[53]
Syagrus romanzoffiana Palm fibers	5, 10, 15, 20	113.89–119.44	1.12×10^{8} to 5.72×10^{8}	$[1-(1-\alpha)^{1/3}]^2$	[54]
Date seeds	10, 20, 30, and 40	170–190	13.8×10^{12}	$[(1-\alpha)^{-1/3}-1]^2$	[57]
Pine and corn starch pellet	5, 10, 20, and 50	218.05	1.28×10^{14}	$1-(1-\alpha)^{1/3}$	[58]

random nucleation and growth mechanisms indicates diffusion-limited behavior, which is highly relevant for scaling fixed-bed and fluidized-bed reactors where heat and mass transfer govern efficiency. The calculated activation energies (47.7–239.8 kJ/mol) and mean enthalpy (~55 kJ/mol) quantify the external energy required to initiate and sustain pyrolysis, supporting energy balance calculations and optimized heating strategies. The consistently positive Gibbs free energy values confirm that continuous energy input is necessary, underscoring the importance of integrating pyrolysis with energy recovery options such as syngas combustion, co-pyrolysis, or waste-heat utilization. Together, these results bridge laboratory-scale kinetics with industrial practice, highlighting DdwFs as a viable feedstock for renewable biofuel production and system integration.

The predominance of random nucleation and growth models (M15–M22) indicates that DdwF pyrolysis follows diffusion-limited pathways. This mechanistic behavior is highly relevant for industrial applications, as it implies that reactor performance will depend on particle size, bed configuration, and mixing efficiency. In fixed-bed or fluidized-bed systems, ensuring uniform heat transfer and minimizing diffusion limitations will be critical to achieving complete conversion. Our findings therefore not only identify the kinetic triplet of DdwFs but also provide mechanistic insight into how these fibers behave under scaled-up pyrolysis conditions.

Conclusion

This study investigated the pyrolysis behavior of *Dracaena draco* waste fibers (DdwFs) at heating rates of 15, 25, and 30 °C/min using thermogravimetric analysis and the Coats–Redfern method. The results revealed that DdwFs undergo multi-step degradation associated with hemicellulose, cellulose, and lignin decomposition, with random nucleation and growth models (M15, M20, M21, M22) providing the best fit to the process. The calculated activation energies (E_a) ranged from 47.7 to 239.8 kJ/mol, and thermodynamic analysis confirmed that pyrolysis is endothermic and non-spontaneous, requiring external energy input. These kinetic and thermodynamic parameters offer valuable insights for reactor scale-up and heating strategies, contributing to improved energy efficiency in biomass conversion systems.

From an application perspective, valorization of DdwFs represents a sustainable pathway to reduce agricultural and landscape waste while producing renewable energy. Industrially, integrating DdwFs pyrolysis into biofuel supply chains could reduce fossil fuel dependence and mitigate greenhouse gas emissions.

Looking forward, further work should:

- Couple kinetic and thermodynamic data with life-cycle assessment (LCA) to evaluate long-term sustainability.
- Conduct syngas and bio-oil analyses to optimize fuel yields and composition.
- Characterize biochar properties for applications in soil improvement, carbon sequestration, and advanced functional materials.
- Apply model-free approaches (FWO and KAS) as complementary tools to validate and expand the kinetic analysis of *Dracaena draco* pyrolysis.

Overall, this research highlights DdwFs as a promising feedstock for renewable biofuel production and lays the groundwork for bridging laboratory-scale results with industrial bioenergy applications.

Funding

The authors thankful to United Arab Emirates University for funding this work through Fund Code: 12R287 and 12R301.

CRediT authorship contribution statement

Abdelwaheb Hadou: Writing – original draft, Validation, Resources, Methodology, Conceptualization. **Ahmed Belaadi:** Writing – review & editing, Supervision, Resources, Methodology, Investigation. **Aghilas Brahmi:** Writing – review & editing, Validation. **Messaouda Boumaaza:** Writing – review & editing, Validation. **Mohammad Jawaid:** Writing – review & editing, Visualization, Validation. **Djamel Ghernaout:** Writing – review & editing, Validation. **Vincenzo Fiore:** Writing – review & editing, Validation.

Declaration of competing interest

The authors declare that they have no known competing financial interests or personal relationships that could have appeared to influence the work reported in this paper.

Data availability

Data will be made available on request.

References

[1] Taşar Ş. Thermal conversion behavior of cellulose and hemicellulose fractions isolated from tea leaf brewing waste: kinetic and thermodynamic evaluation. Biomass Convers Biorefin 2022;12(7):2935–47. https://doi.org/10.1007/s13399-021-01697-2.

[2] S. Sarıdemir, F. Polat, H. Simsir, C. Uysal, et Ü. Ağbulut, « Novel green hydrochar production for renewable fuel substitutes, and experimental investigation of its usability on CI engine performance, combustion, and emission characteristics », *Energy*, p. 134530, 2025, doi: doi:10.1016/j.energy.2025.134530.

[3] Mian I, et al. Kinetic study of biomass pellet pyrolysis by using distributed activation energy model and Coats Redfern methods and their comparison. Bioresour Technol 2019;294:122099. https://doi.org/10.1016/j.biortech.2019.122099.

[4] An W, Tang Y, Liang K, Cai M, Wang T, Wang Z. Study on temperature distribution and CO diffusion induced by cable fire in L-shaped utility tunnel. Sustain Cities Soc 2020;62:102407. https://doi.org/10.1016/j.scs.2020.102407.

[5] An W, Yin X, Cai M, Gao Y, Wang H. Influence of vertical channel on downward flame spread over extruded polystyrene foam. Int J Therm Sci 2019;145:105991. https://doi.org/10.1016/j.ijthermalsci.2019.105991.

[6] T. Ozawa, « A New Method of Analyzing Thermogravimetric Data », *Bulletin of the Chemical Society of Japan*, vol. 38, n° 11, p. 1881-1886, nov. 1965, doi: 10.1246/bcsj.38.1881.

[7] A. W. Coats et J. P. Redfern. Kinetic Parameters from Thermogravimetric Data. Nature 1964;201(4914):68–9. https://doi.org/10.1038/201068a0.

[8] Ferfari O, Belaadi A, Bourchak M, Ghernaout D, Ajaj RM, Chai BX. Thermal decomposition of Syagrus romanzoffiana palm fibers: Thermodynamic and kinetic studies using the coats-redfern method. Renew Energy 2024;231:120928. https://doi.org/10.1016/j.renene.2024.120928.

[9] A. Khan *et al.*, « Analysis of thermal decomposition kinetics of chicken feather fiber reinforced Poly-lactic acid composites filament », *Heliyon*, vol. 10, n° 2, 2024, doi: 10.1016/j.heliyon.2024.e24245.

[10] Luo S, Xiao B, Hu Z, Liu S. Effect of particle size on pyrolysis of single-component municipal solid waste in fixed bed reactor. Int J Hydrogen Energy 2010;35(1):93–7. https://doi.org/10.1016/j.ijhydene.2009.10.048.

[11] Y. El may, M. Jeguirim, S. Dorge, G. Trouvé, et R. Said. Study on the thermal behavior of different date palm residues: Characterization and devolatilization kinetics under inert and oxidative atmospheres. Energy 2012;44(1):702–9. https://doi.org/10.1016/j.energy.2012.05.022.

[12] Elmay Y, Jeguirim M, Trouvé G, Said R. « Kinetic analysis of thermal decomposition of date palm residues using Coats-Redfern method », *Energy sources*. Part a: Recovery, Utilization and Environmental Effects 2016;38(8):1117–24. https://doi.org/10.1080/15567036.2013.821547.

[13] I. Lalaymia, A. Belaadi, H. Alshahrani, D. Ghernaout, et H. Mukalazi, « Sustainable Renewable Biofuel Production Toward Pyrolysis of Fibers Biowaste Agave Americana L. and Thermodynamics Mechanisms Kinetic Parameters Triplet Assessment », *Journal of Natural Fibers*, vol. 22, n° 1, p. 2537069, déc. 2025, doi: 10.1080/15440478.2025.2537069.

[14] O. Ferfari, A. Belaadi, H. Alshahrani, D. Ghernaout, et H. Mukalazi, « Unraveling the Pyrolysis Mechanisms of *Syagrus* Palm Waste Fibers Through Gaussian Deconvolution and Kinetic Modeling », *Journal of Natural Fibers*, vol. 22, n° 1, p. 2562473, déc. 2025, doi: 10.1080/15440478.2025.2562473.

[15] A. H. Supee et M. A. A. Zaini, « Kinetics, thermodynamics, and thermal decomposition behavior of palm oil empty fruit bunch, coconut shell, bamboo, and cardboard pyrolysis: an integrated approach using Coats–Redfern method », *Environ Monit Assess*, vol. 195, n° 10, p. 1218, oct. 2023, doi: 10.1007/s10661-023-11866-7.

[16] A. Hadou, A. Belaadi, H. Alshahrani, et M. K. A. Khan, « Extraction and characterization of novel cellulose fibers from Dracaena draco plant », *Materials Chemistry and Physics*, vol. 313, p. 128790, févr. 2024, doi: 10.1016/j.matchemphys.2023.128790.

[17] T. Raja, « Exploring a natural fiber extracted from *henequen* plant leaves: A sustainable innovation for reinforcement in composite materials », *Results in Engineering*, vol. 25, p. 104015, mars 2025, doi: 10.1016/j.rineng.2025.104015.

[18] S. Atoui, A. Belaadi, B. Xian, M. M. S. Abdullah, A. Al-khawlani, et D. Ghernaout, « International Journal of Biological Macromolecules Extracting and characterizing

novel cellulose fibers from Chamaerops humilis rachis for textiles ' sustainable and cleaner production as reinforcement for potential applications », *International Journal of Biological Macromolecules*, n° July, p. 134029, 2024, doi: 10.1016/j.ijbiomac.2024.134029.

[19] A. Hadou, A. Belaadi, D. Ghernaout, et H. Mukalazi, « Forecasting the Thermal Degradation Depending on the Kinetics of Dracaena Draco Lignocellulosic Fibers Using an Artificial Neural Network », *Journal of Natural Fibers*, vol. 22, n° 1, p. 2531368, déc. 2025, doi: 10.1080/15440478.2025.2531368.

[20] O. Ferfari, A. Belaadi, D. Ghernaout, et M. I. Ammarullah, « Thermogravimetric Analysis and Artificial Neural Network Modeling of *Syagrus Romanzoffiana* Bio-Fibers: A Comparative Study of Kinetic and Thermodynamic Parameters Using Model-Free Methods », *Journal of Natural Fibers*, vol. 22, n° 1, p. 2549912, déc. 2025, doi: 10.1080/15440478.2025.2549912.

[21] A. Hadou, A. Belaadi, I. M. H. Alshaikh, et D. Ghernaout, « Pyrolysis features of Dracaena draco lignocellulosic fibers: Kinetic and thermodynamic analysis at various heating rates through coats-redfern method », *Case Studies in Thermal Engineering*, vol. 64, p. 105406, déc. 2024, doi: 10.1016/j.csite.2024.105406.

[22] Mishra A, et al. A comparative study on pyrolysis kinetics and thermodynamic parameters of little millet and sunflower stems biomass using thermogravimetric analysis. Prospecting Pecan Nutshell Pyrolysis as a Source of Bioenergy and Bio-Based Chemicals Using Multicomponent Kinetic Modeling, Thermodynamic Parameters Estimation, and Py-GC/MS Analysis 2023;367:128231. https://doi.org/10.1016/j.biortech.2022.128231.

[23] I. Lalaymia, A. Belaadi, et D. Ghernaout, « Studying Gaussian deconvolution and multicomponent kinetics models in *Agave* cellulosic fibers pyrolysis: Application in sustainable bioenergy for cleaner production », *Biomass and Bioenergy*, vol. 192, p. 107488, janv. 2025, doi: 10.1016/j.biombioe.2024.107488.

[24] Lalaymia I, Bedjaoui A, Belaadi A, Abdullah MM, Ghernaout D, Al-Khawlani A. Slow pyrolysis of Agave americana L. fibers: Analysis of kinetics and thermodynamics using the coats-redfern method at different heating rates. Ind Crop Prod 2024;219:119043. https://doi.org/10.1016/j.indcrop.2024.119043.

[25] M. Asif, M. Bilal, et A. Rauf, « Investigation of Kinetic and Thermodynamic Parameters of Sapodilla Leaves Pyrolysis Using Coats Redfern Model », 2024.

[26] R. Zhou, B. Huang, Y. Ding, W. Li, et J. Mu, « Thermal decomposition mechanism and kinetic study of plasticwaste chlorinated polyvinyl chloride », *Polymers*, vol. 11, n° 12, 2019, doi: 10.3390/polym11122080.

[27] M. Pigłowska, B. Kurc, Ł. Rymaniak, P. Lijewski, et P. Fuć, « Kinetics and thermodynamics of thermal degradation of different starches and estimation the OH group and H2O content on the surface by TG/DTG-DTA », *Polymers*, vol. 12, n° 2, 2020, doi: 10.3390/polym12020357.

[28] Z. A. Hussein, Z. M. Shakor, M. Alzuhairi, et F. Al-Sheikh, « Kinetic and Thermodynamic Study of the Pyrolysis of Plastic Waste », *Environmental Processes*, vol. 10, n° 2, 2023, doi: 10.1007/s40710-023-00640-z.

[29] Kumar M, Mishra PK, Upadhyay SN. Thermal degradation of rice husk: effect of pre-treatment on kinetic and thermodynamic parameters. Fuel 2020;268:117164. https://doi.org/10.1016/j.fuel.2020.117164.

[30] S. Sobek et S. Werle. Kinetic modelling of waste wood devolatilization during pyrolysis based on thermogravimetric data and solar pyrolysis reactor performance. Fuel 2020;261:116459. https://doi.org/10.1016/j.fuel.2019.116459.

[31] M. Ali *et al.*, « Thermal Analyses of Loose Agave, Wheat Straw Fibers and Agave/Wheat Straw as New Hybrid Thermal Insulating Materials for Buildings », *Journal of Natural Fibers*, vol. 18, n° 12, p. 2173-2188, déc. 2021, doi: 10.1080/15440478.2020.1724232.

[32] Torres-Sciancalepore R, et al. Synergistic effects of the mixing factor on the kinetics and products obtained by co-pyrolysis of Rosa rubiginosa rosehip seed and husk wastes. Energ Conver Manage 2024;302:118095.

[33] Torres-Sciancalepore R, et al. Assessment of the behavior of Rosa rubiginosa seed waste during slow pyrolysis process towards complete recovery: Kinetic modeling and product analysis. Energ Conver Manage 2022;272:116340.

[34] Naqvi SR, Ali I, Nasir S, S. Ali Ammar Taqvi, A. E. Atabani, et W.-H. Chen. Assessment of agro-industrial residues for bioenergy potential by investigating thermo-kinetic behavior in a slow pyrolysis process. Fuel 2020;278:118259. https://doi.org/10.1016/j.fuel.2020.118259.

[35] Rasam S, Moshfegh Haghighi A, Azizi K, Soria-Verdugo A, M.. Keshavarz Moraveji, « Thermal behavior, thermodynamics and kinetics of co-pyrolysis of binary and ternary mixtures of biomass through thermogravimetric analysis ». Fuel 2020;280:118665. https://doi.org/10.1016/j.fuel.2020.118665.

[36] Barzegar R, Yozgatligil A, Olgun H, Atimtay AT. TGA and kinetic study of different torrefaction conditions of wood biomass under air and oxy-fuel combustion atmospheres. J Energy Inst 2020;93(3):889–98. https://doi.org/10.1016/j.joei.2019.08.001.

[37] Agnihotri N, Gupta GK, Mondal MK. Thermo-kinetic analysis, thermodynamic parameters and comprehensive pyrolysis index of Melia azedarach sawdust as a genesis of bioenergy. Biomass Convers Biorefin 2024;14(2):1863–80. https://doi.org/10.1007/s13399-022-02524-y.

[38] Ma J, et al. Pyrolysis kinetics and thermodynamic parameters of the hydrochars derived from co-hydrothermal carbonization of sawdust and sewage sludge using thermogravimetric analysis. Bioresour Technol 2019;282:133–41. https://doi.org/10.1016/j.biortech.2019.03.007.

[39] Jiang L, et al. Pyrolytic behavior of waste extruded polystyrene and rigid polyurethane by multi kinetics methods and Py-GC/MS. Fuel 2018;222:11–20. https://doi.org/10.1016/j.fuel.2018.02.143.

[40] Chen R, Li Q, Zhang Y, Xu X, Zhang D. Pyrolysis kinetics and mechanism of typical industrial non-tyre rubber wastes by peak-differentiating analysis and multi kinetics methods. Fuel 2019;235:1224–37. https://doi.org/10.1016/j.fuel.2018.08.121.

[41] Vyazovkin S, Burnham AK, Criado JM, Pérez-Maqueda LA, Popescu C, Sbirrazzuoli N. ICTAC Kinetics Committee recommendations for performing kinetic computations on thermal analysis data. Thermochim Acta 2011;520(1):1–19. https://doi.org/10.1016/j.tca.2011.03.034.

[42] R. Chen, Q. Li, X. Xu, et D. Zhang, « Pyrolysis kinetics and reaction mechanism of representative non-charring polymer waste with micron particle size », *Energy Conversion and Management*, vol. 198, n° May, p. 111923, 2019, doi: 10.1016/j.enconman.2019.111923.

[43] V. N. Zikhali, C. Mpofu, D. Nyama, B. Nyoni, et K. Mushonga, «Kinetic and Thermodynamic Analysis of Chicken Manure Pyrolysis for Sustainable Waste Management in the Poultry Industry Kinetic and Thermodynamic Analysis of Chicken Manure Pyrolysis for Sustainable Waste Management in the Poultry Industry», n° August, 2023, doi: 10.36348/sijcms.2023.v06i06.003.

[44] Tariq R, et al. Kinetic and thermodynamic evaluation of pyrolysis of jeans waste via coats-redfern method. Korean J Chem Eng 2023;40(1):155–61. https://doi.org/10.1007/s11814-022-1248-3.

[45] A. Khawam et D. R. Flanagan, « Solid-State Kinetic Models: Basics and Mathematical Fundamentals », *The Journal of Physical Chemistry B*, vol. 110, n° 35, p. 17315-17328, sept. 2006, doi: 10.1021/jp062746a.

[46] Sun S, Yuan Y, Chen R, Xu X, Zhang D. Kinetic, thermodynamic and chemical reaction analyses of typical surgical face mask waste pyrolysis. Therm Sci Eng Prog 2021;vol. 26, no October:101135. https://doi.org/10.1016/j.tsep.2021.101135.

[47] Zou H, Evrendilek F, Liu J, Buyukada M. Combustion behaviors of pileus and stipe parts of Lentinus edodes using thermogravimetric-mass spectrometry and Fourier transform infrared spectroscopy analyses: thermal conversion, kinetic, thermodynamic, gas emission and optimization analyses. Bioresour Technol 2019;288:121481. https://doi.org/10.1016/j.biortech.2019.121481.

[48] Zhang J, et al. Kinetics, thermodynamics, gas evolution and empirical optimization of cattle manure combustion in air and oxy-fuel atmospheres. Appl Therm Eng 2019;149:119–31. https://doi.org/10.1016/j.applthermaleng.2018.12.010.

[49] Huang H, Liu J, Liu H, Evrendilek F, Buyukada M. Pyrolysis of water hyacinth biomass parts: Bioenergy, gas emissions, and by-products using TG-FTIR and Py-GC/MS analyses. Energ Conver Manage 2020;207:112552. https://doi.org/10.1016/j.enconman.2020.112552.

[50] Naqvi SR, et al. Synergistic effect on co-pyrolysis of rice husk and sewage sludge by thermal behavior, kinetics, thermodynamic parameters and artificial neural network. Waste Manag 2019;85:131–40. https://doi.org/10.1016/j.wasman.2018.12.031.

[51] A. Petrovič *et al.*, « Thermo-kinetic analysis of pyrolysis of thermally pre-treated sewage sludge from the food industry », *Thermal Science and Engineering Progress*, vol. 42, n° January, 2023, doi: 10.1016/j.tsep.2023.101863.

[52] Ferfari O, Belaadi A, Bourchak M, Ghernaout D, Ajaj RM, Chai BX. Thermal Decomposition of Syagrus romanzoffiana Palm Fibers: Thermodynamic and Kinetic Studies using the Coats-Redfern Method. Renew Energy 2024:120928. https://doi.org/10.1016/j.renene.2024.120928.

[53] Raza M, Abu-Jdayil B, Inayat A. Pyrolytic kinetics and thermodynamic analyses of date seeds at different heating rates using the Coats–Redfern method. Fuel 2023;342(December):2022. https://doi.org/10.1016/j.fuel.2023.127799.

[54] Tabal A, Barakat A, Aboulkas A, K.. El harfi, « Pyrolysis of ficus nitida wood: Determination of kinetic and thermodynamic parameters ». Fuel 2021;283:119253. https://doi.org/10.1016/j.fuel.2020.119253.